In vivo chemical investigation of human skin using a confocal Raman fiber optic microprobe

L. Chrit
L'Oréal Recherche
Aulanay sous Bois
France
and
Unité Médian CNRS UMR 6142
UFR Pharmacie, IFR 53
Université de Reims Champagne-Ardenne
51 rue Cognacq-Jay
51096 Reims Cedex, France

C. Hadjur
L'Oréal Recherche
Aulnay sous Bois
France
E-mail: chadjur@rd.loreal.com

S. Morel
Horiba Jobin Yvon S.A.S.
Division Raman
231 rue de Lille
59650 Villeneuve d'Ascq
France

G. Sockalingum
Unité Médian CNRS UMR 6142
UFR Pharmacie
IFR 53
Université de Reims Champagne-Ardenne
51 rue Cognacq-Jay
51096 Reims Cedex, France

G. Lebourdon
Horiba Jobin Yvon S.A.S.
Division Raman
231 rue de Lille
59650 Villeneuve d'Ascq
France

F. Leroy
L'Oréal Recherche
Aulnay sous Bois
France

M. Manfait
Unité Médian CNRS UMR 6142
UFR Pharmacie, IFR 53
Université de Reims Champagne-Ardenne
51 rue Cognacq-Jay
51096 Reims Cedex, France

Abstract. To evaluate the potential of a new *in vivo* confocal Raman microprobe, we undertake a pilot study in human skin. A fiber optic probe is operated with a 633-nm laser and trials are conducted in healthy volunteers. We examine changes in molecular composition and structure of the *stratum corneum*, from different volunteers, from different anatomical sites and skin layers. Main spectral variations are detected in the following regions: 800 to 900 cm^{-1} (amino acids); 1200 to 1290 cm^{-1} (proteins); and 1030 to 1130 cm^{-1}, 1300 to 1450 cm^{-1}, and 2800 to 2900 cm^{-1} (lipids). Curve fitting of the amide 1 region performs in detail protein secondary structural variations of the amide 1 band. Protein conformation is also found to vary depending on the anatomical site and volunteer. Similar analysis of the 730- to 1170-cm^{-1} spectral window reveals a different organization of lamellar lipids: gel for forearm and palm, and liquid-crystalline phase for fingertips. All these variations result from changes in the *stratum corneum* components such as natural moisturizing factor (NMF), lipids (namely ceramides), and water. Hierarchical clustering classification is also performed to sort out Raman data obtained from different subjects. Further improvement of the confocal probe would be to adapt a 360-deg configuration enabling access to other anatomical sites. [DOI: 10.1117/1.2003747]

Keywords: *in vivo* confocal Raman microprobe; noninvasive; human skin; natural moisturizing factor; lipid structure; protein structure; water content.

Paper 05005R received Jan. 10, 2005; revised manuscript received Apr. 9, 2005; accepted for publication Apr. 12, 2005; published online Aug. 30, 2005.

1 Introduction

The skin is a heterogeneous organ made of tissues and layers that differ in morphology and molecular composition. The upper, epithelial tissue is the epidermis. The underlying dermis is a connective tissue. The dermis varies in thickness from 1 to 4 mm. The thickness of covering epidermis can vary from 40 μm up to 1 mm on the palms and is stratified. The uppermost layers contain cornifying cells called corneocytes. As a whole, they make the thin horny layer called *stratum corneum*, the ultimate barrier between the organism and the external environment. Obviously, the *stratum corneum* (SC) plays a key role not only in protecting and preventing against external aggressions, but in regulating of water flux in and out as well. The *stratum corneum* ranges from 10 to 15 μm thick, except for the palmo-plantar area, where it can be about ten times thicker. These functions are fulfilled by a unique structure consisting of 10 to 15 layers of flattened, anucleated, keratinized cells embedded in lipids matrix, such as "bricks in

Address all correspondence to Christophe Hadjur, Physics, L'Oréal Recherche, 1, avenue Eugene Schueller – BP 22, Aulnay Sous Bois Cedex, 93601 France. Tel: +33 1 48 68 99 90. Fax: +33 1 58 31 70 65. E-mail: chadjur@rd.loreal.com

1083-3668/2005/10(4)/044007/11/$22.00 © 2005 SPIE

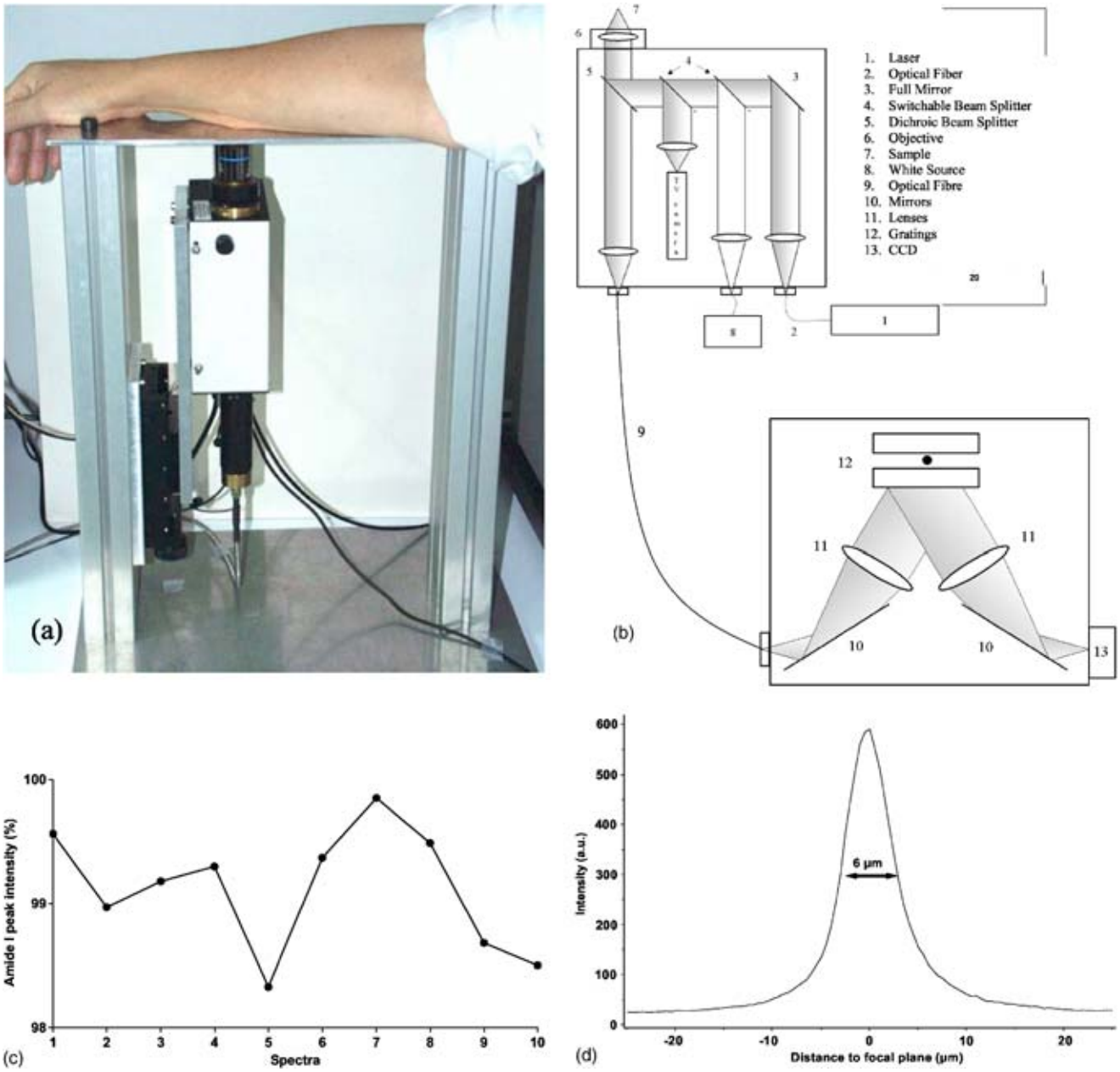

Fig. 1 (a) Picture of the *in vivo* confocal Raman fiber optic microprobe in the configuration for investigating the forearm. The mount contains a metal ring with a hole of about 1 mm in diameter. This hole avoids or limits the motion of the subject during the measurements and thus stabilizes the whole system. (b) Representation of the schematic illustrating the light path of the system, (c) the reproducibility of the spectra, and (d) the axial resolution. The easy handling of this microprobe allows access to other parts of the body.

mortar"[1] or more sophistically corneocyte cells surrounded by a 3-D multilamellar lipid domain.[2,3] In general, molecular composition of SC is: 75 to 80% fibrous protein (mostly in α-keratin conformation),[4,5] 5 to 10% lipids (ceramides, cholesterol, and fatty acids), and 5 to 10% of other materials (amino acids, NME, etc.).[6]

Several biophysical techniques have been developed during the last decade to improve skin description and knowledge, driven by medical, pharmaceutical, and cosmetic research.[7] Vibrational spectroscopic techniques, such as infrared absorption and Raman scattering, are among such approaches that have emerged in this direction. Indeed, they give detailed information on molecular structure, composition, and microenvironment. Infrared (IR) absorption spectroscopy has been used for *in vivo* studies of *stratum corneum* hydration and permeability.[8–12] However, due to the strong absorption of mid- and far-infrared radiation by water, the penetration depth in naturally hydrated tissue such as the skin is limited to a few microns. Therefore, in an *in vivo* IR-spectroscopic experiment, only the outermost layer of the *stratum corneum* is sampled.

Raman spectroscopy is a complementary technique to infrared and provides molecular, structural, and compositional information of the sample. Nevertheless, in the confocal

mode, it has the advantage of providing information from the surface of the skin down to several microns deep into the skin. This noninvasive and nondestructive technique can be operated without contact, does not require sample preparation, and shows great potential for the study of biological tissues. Early studies aimed at tissue characterization and pathological tissue classification, many of them targeting the skin.[4,13–17] The first *in vivo* studies of human skin using Raman spectroscopy were reported by Williams et al.[13] Schrader et al.,[15] and Shim and Wilson.[16] The availability of *in vivo* confocal devices allowed enhancing in-depth measurements of the skin from the surface to several microns below the skin surface.[17–19] This technique therefore provides a straightforward way to get more insights into the chemical structure and physical behavior of upper skin layers.

This preliminary work was carried out on healthy individuals using a newly developed *in vivo* confocal Raman microprobe operating with an optic fiber and a 633-nm laser. This probe permits acquisition of the spectrum over the whole frequency range from 500 to 3600 cm^{-1}. Therefore, information about the fingerprint region and the higher frequencies containing water vibrations (2800 to 3600 cm^{-1}) are collected simultaneously without using two different wavelengths as previously reported.[19] Our study aimed at demonstrating the feasibility of the new probe in evaluating skin *in vivo*. Skin composition and structure variations were examined and discussed from *in vivo* Raman spectra of human skin from healthy volunteers. Data from several spots in the same area, variations between different anatomical sites, various volunteers, and different layers were compared. Skin hydration was also considered.

2 Material and Methods

2.1 *Experimental Device*

The equipment included a fiber-coupled dispersive Raman spectrograph (InduRAM, Horiba Jobin Yvon, France) and a confocal Raman probe (Conf Head, Horiba Jobin Yvon, France). The objective used in this experiment was a 50× long working distance lens (Olympus, Japan), with a numerical aperture of 0.5, operating in air. In our cosmetics application, it is necessary to work with this type of objective lens instead of an oil or water immersion lens, which is in contact with the skin. A piezo-electric device (Physics Instrument, Germany) allowed us to control high-precision axial translation of the lens throughout depth profiling from the surface down to a defined depth within the skin. This scanning device was directly controlled by the data acquisition software (LabSpec, Horiba Jobin Yvon, France), allowing automated depth profiling procedures.

The excitation source was a 633-nm He–Ne laser (Melles Griot, USA), delivering about 3.5 mW at sample level. The spectrograph was equipped with an air-cooled CCD detector (Wright Instrument, UK), with a chip size of 1024 × 256, and a 600-gr/mm grating, which allows the covering of a large spectral range from 500 to 3600 cm^{-1} in a single shot acquisition with a spectral resolution of about 7 cm^{-1}, which is conserved at deeper regions. The acquisition time was about 20 s, which enabled us to perform rapid measurements at the surface as well as in deeper layers. A color video camera integrated within the probe enabled the user to visualize the sample in reflexion. Insertion of a density filter on the laser path allowed us to avoid any saturation of the camera due to the diffusion of the laser on the skin. The device also permitted us to visualize the attenuated laser spot focused on the sample, and therefore to achieve an accurate positioning of the laser on the sample. The compact design and the ease of handling the fiber optic probe also offer other possibilities such as access to other parts of the body, which stands as the very unique feature of this setup.

The main sampling difficulties arising from *in vivo* conditions result from body movements, heart beat disturbances, and laser heating effects, which all affect the laser focal point. However, in the present case, the laser heating effects were negligible due to the low laser power at the sample level. To optimize the sampling conditions by limiting body motions and heart-beat-induced disturbances, the device was first stabilized using an inverted setup [see Fig. 1(a)]. A schematic of the system to better understand the light path is illustrated in Fig. 1(b). The investigated part of the body was pressed against a holder, in which a small hole had been drilled to perform measurements. Hence, skin was flattened near the measured area so that large motions and therefore defocusing interferences were avoided. The interest of using a small aperture rather than a window placed between the lens and the sample (as reported by Caspers et al.)[19] not only lies in avoiding interferences of Raman features generated by the window material itself, but also in limiting the refraction index effects induced by an additional interface, which might affect the spatial and namely axial resolution. Data reproducibility was experimentally checked by recording ten successive spectra at the skin surface, showing very slight spectral features and intensity variations of less than 5% [see Fig. 1(c)].

Visible light excitation at 633 nm was preferred because quantum efficiency (and therefore sensitivity) of charge coupled device (CCD) detectors rapidly decreases above 850 nm and becomes blind beyond 1100 nm. However, at 633 nm, one benefits from the maximum sensitivity of such detection devices over the whole spectrum, giving optimal access to both low and high frequency regions, the latter being important for water content analysis. Nevertheless, using near-infrared (NIR) excitations may be of interest when facing fluorescence background interferences generated by applying cosmetic or pharmaceutical products on skin that turn out to be strongly fluorescent. Yet, one should bear in mind that going further to the infrared domain leads to weaker Raman scattering efficiency (as Raman intensity is directly proportional to $1/\lambda^4$) and high power laser sources are thus required.

2.2 *Determination of Axial Resolution*

The confocality principle is based on the selection of a restricted collection volume, often using a small aperture. This considerably improves lateral and depth resolution by filtering out the signal coming from out-of-focus or adjacent regions. Another advantage lies in a significant reduction of fluorescent background generated by the regions surrounding the laser focus point. These two advantages, namely high axial discrimination and fluorescence reduction, played a determining role in obtaining good quality Raman data, both from skin surface and from deeper layers.

The depth of field of the objective used was directly related to the volume sampled and was determined experimentally. For this evaluation, a silicon sample was moved through the laser focus and the Raman collected signal was measured. Raman spectra of silicon were measured using the long working distance 50× objective, at 0.5 μm depth increments, from 25 μm above the surface to 25 μm in depth. The area of the Raman peak associated to the Si–Si vibrational mode at 520 cm^{-1} was plotted against the position of the laser focus, and the axial resolution was inferred from the full width at half maximum (FWHM) of this response curve. Under the conditions of the study, FWHM was found to be about 6 μm. This is illustrated in Fig. 1(d).

2.3 *Sample*

The *in vivo* experiments were performed on seven healthy volunteers (28 to 60 years old), including two males and five females. The measurements were conducted at different anatomical sites: the fingertip (index, major, right and left hands), the thenar or palm, and the forearm. Before each measurement, the skin was cleaned with a single wipe of tissue soaked in 97% ethanol. For each individual and each site, three spectra from different points were averaged. The collection times varied about 20 s and depended on the subject. The spectra were measured at a range of depths below the skin surface with depth increments of 4 μm for the profile of the arm and the hand. Considering the optical deconvolution and the oversampling, a step smaller than the axial resolution can be used.

2.4 *Data Analysis*

2.4.1 *Data preprocessing*

All spectra were acquired and preprocessed according to the following scheme: linear baseline substraction (to get rid of the intrinsic skin fluorescence); and normalizing bands, respectively, at 1450 cm^{-1} (which corresponds to the common band of lipids and proteins in the *stratum corneum*) for the range 400 to 2000 cm^{-1}, and at 2940 cm^{-1} for the range 2800 to 3600 cm^{-1}.[14] The normalization is based on the integration of the area under the curve from 1445 to 1455 cm^{-1} and between 2935 to 2945 cm^{-1}. This normalization is scaled to have a standard deviation of 1. All these functions, together with the averaging procedure, were performed using the data acquisition software (LabSpec, Horiba Jobin Yvon, France).

2.4.2 *Cluster analysis*

Cluster analysis was performed on the average spectra collected from the same anatomical site of different subjects, using the fingerprint region 600 to 1700 cm^{-1}. The spectral classification is based on the spectral characteristics of the skin available from different subjects. The result of the cluster analysis is a dendogram that was calculated using Ward's algorithm and Euclidean distance available in the OPUS software (Bruker Optics, Wissembourg, France).

2.4.3 *Curve-fitting of Raman spectra*

When the natural bandwidth is greater than the adjacent peak-to-peak separation, it is difficult to observe resolved features of overlapping Raman bands. The problem cannot be solved by increasing instrument resolution. To gain more insight into the overlapping structures, some mathematical processes can be applied to extract the hidden structural information from the spectra. Fourier deconvolution, second derivatives, and curve fitting are some of the currently used methods.[20] The curve-fitting method was used on two spectral windows: 730 to 1170 cm^{-1} and 1600 to 1700 cm^{-1} after area normalization and second derivative for the peak selection. The curve-fitting procedure used was based on a least-square method using Gaussian and Lorentzian bands.[20] This procedure calculates a theoretical spectrum that best fits the experimental one. The accuracy of the fit is given by the chi-square (χ^2) value. The lower the value of the chi square, the better it fits.[21]

3 Results

The main spectral features of the human *stratum corneum* obtained with our fiber microprobe are assigned and described in Table 1. No visual or spectral changes are observed during the measurements, which would indicate degradation or heating of the sample. The fiber optic probe operates with a 633-nm laser and tests were conducted on healthy volunteers. We described earlier changes in *in vivo* Raman spectra between different spots of the same area, different anatomical sites, different individuals, and different skin layers.

3.1 *Variations between Different Spots in the Same Site and Different Anatomical Sites in a Single Subject*

Figure 2 shows *in vivo* Raman spectra of different spots of the fingertip (same site) from the same subject. Some variations of intensity can be noticed as well as slight changes in molecular composition. These variations concern amino acid composition, for instance at 642 cm^{-1} (tyrosine), at 855 cm^{-1} [δ(CCH) aromatic], and a NMF constituent [885 cm^{-1} vibration from the pyrrolidone-5-carboxylic acid (PCA)]. So, this analysis only reveals slight differences within the same site.

In vivo Raman spectra at different anatomical regions are shown in Fig. 3. The spectra were recorded from the fingertip of the middle finger, the thenar (ball of the hand), and the volar aspect of the forearm. All spectra represent the average of several recordings per measurement spot. Site selection was made considering the ergonomics of the device, which means based on easy accessibility. Furthermore, the thickness and the functionality of the *stratum corneum* vary widely in tested areas. For example, the *stratum corneum* of the volar aspect of the forearm is very thin, about 10 to 15 μm, whereas the *stratum corneum* of the fingertip or hand palm is much thicker (about ten times), due to the high frictional forces it has to withstand. In all the *stratum corneum* spectra extracted from various anatomical sites, we observed that the amide 1 and amide 3 vibrations are located around 1655 cm^{-1} and 1270 cm^{-1}, respectively, indicating the helical conformation of the major protein previously described for skin.[22,14] In addition, the presence of the variation around 935 cm^{-1} confirmed this observation (Fig. 3). The *stratum corneum* spectral signatures taken at different anatomical sites display several differences in the amide 1 region, the amide 3 region, and the band 1420 cm^{-1}, the intensity of the bands 855 and 880 cm^{-1}.

To provide further understanding concerning these variations, especially about the protein secondary structure, we

Table 1 Raman assignment of the major vibrational modes for the human *stratum corneum* updated. δ=deformation; ν=stretch; ρ=rock; str.=stretching. * are revised bands. Values and assignments are resulted from this work and other literature reports.

Wavenumber (cm^{-1})	Assignment
424	δ(CCC) skeletal backbone
526	ν(SS) trans-gauche-gauche*
600	ρ(H) wagging
623	ν(CS), phe ring str.; tyr ring str.*
644	ν(CS); amide 4; tyr
702	cholesterol*
746	$\rho(CH_2)$ in-phase
827	δ(CCH) aliphatic/tyrosine "exposed"*
850	δ(CCH) aromatic/tyrosine "buried"*
883	$\rho(CH_2)$; COC ring sym.; ν(CC); ν(CN); lys*; PCA
939	$\rho(CH_3)$ terminal; ν(CC) α-helix
956	$\rho(CH_3)$; δ(CCH) olefinic
1002	ν(CC) aromatic ring; phe
1031	ν(CC) skeletal conformation; lipid
1062	ν(CC) skeletal trans conformation
1088	ν(CC) skeletal random conformation
1102	$\nu(C\alpha C\beta)$; $\rho(C\beta H3)$; ala (CC str.)*
1126	ν(CC) skeletal trans conformation
1155	ν(CC); δ(COH)
1172	ν(CC)
1207	tyr, phe, amide 3*
1244	δCH_2 wagging; ν(CN) amide 3 disordered
1274	ν(CN) and δ(NH) amide 3 α-helix
1296	$\delta(CH_2)$
1336	—
1385	$\delta(CH_3)$ symmetric
1421	$\delta(CH_3)$; NMF*
1450	$\delta(CH_2)$ scissoring (lipids and proteins)*
1552	δ(NH) and ν(CN) amide 2
1585	ν(C=C) olefinic
1607	ν(C=C) olefinic; phe, tyr*
1652	ν(C=O) amide 1 α-helix
1743	ν(C=O) lipid
1768	ν(COO)
2723	ν(CH) aliphatic
2852	$\nu(CH_2)$ symmetric
2883	$\nu(CH_2)$ asymmetric
2931	$\nu(CH_3)$ symmetric
2958	$\nu(CH_3)$ asymmetric
3060	ν(CH) olefinic
3280	ν(OH) of H_2O

have used a curve-fitting method to decompose the lamellar lipids region 730 to 1170 cm^{-1} and the broad amide 1 band (1600 to 1700 cm^{-1}) (Tables 2 and 3, and Fig. 4). Undeniably, in some cases there is an overlapping of the *stratum corneum* vibrations with another component such as, for instance, water with δ(OH) vibration around 1640 cm^{-1}.

3.1.1 *Curve-fitting analysis of protein*

The analysis of the range 1600 to 1700 cm^{-1}, including the amide 1 band, reveals different secondary conformation of proteins [Fig. 4(a)]. In all three regions, the major protein of the *stratum corneum*, keratin, is mainly in an α-helix conformation (forearm 38%; thenar 53%; fingertip 39%) (Table 2). This technique discloses another band of the protein at 1660 cm^{-1} for the thenar (11%) and the fingertip (33%),

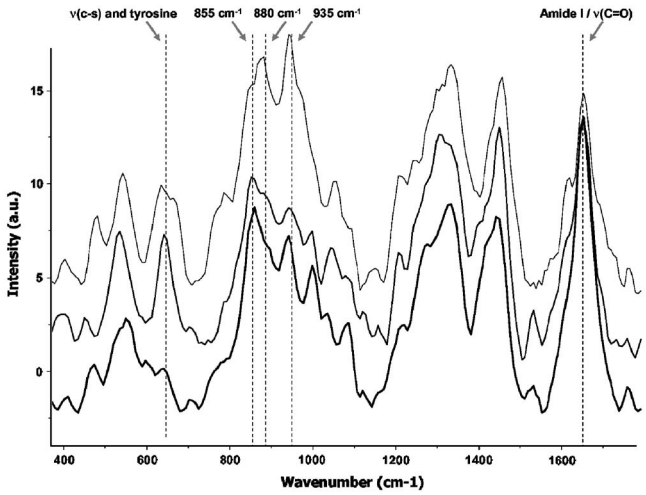

Fig. 2 Raman spectral variability between different spots of the same site: the middle finger tip. The time collection is 20 s per spectrum. Intensity variations and slight molecular variations are observed in this case. Excitation wavelength 633 nm, power at sample is 3.5 mW. The spectra were recorded at the surface of the skin.

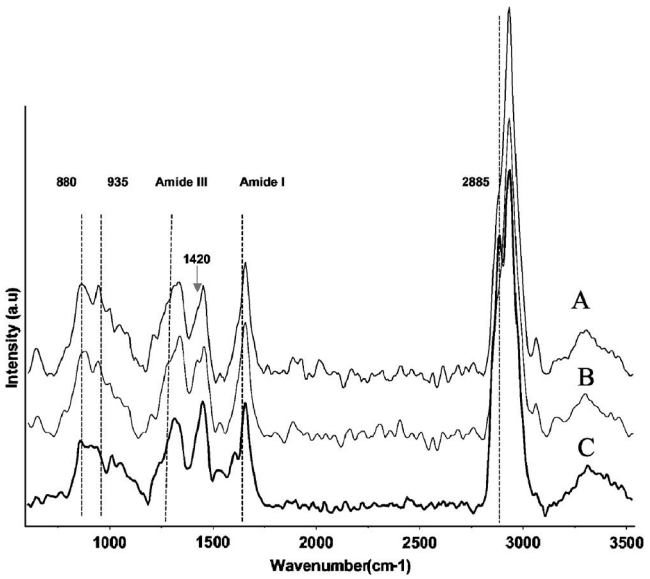

Fig. 3 Comparison of mean spectra obtained at different anatomical sites: (a) fingertip, (b) thenar (ball of the palm of the hand), and (c) forearm. The time acquisition is 20 s per spectrum. (Average of three to six recordings per measurement point.) The spectra were recorded at the surface of the skin.

which corresponds to the random coil conformation of the protein. However, this band is upshifted to higher frequencies 1666 cm^{-1} in the forearm region, which determines the β sheet nature of the protein conformation. We noted that the 1642 cm^{-1} band of water is higher in the thenar region (18%) than in the forearm (10%) or the fingertip (6%) (Table 2). In accordance with the work of Byler and Susi,[23] we can identify the low-frequency component around 1632 cm^{-1} to "out of phase" beta-components of protein. At last, we identify the last band at 1612 cm^{-1}, which is assigned to ν(CC) of aromatic amino acids (phenylalanine, tyrosine).[24]

3.1.2 *Curve analysis of lipids and NMF*

We use 12 bands for the curve fitting of this region [see Fig. 4(b)], which includes the characteristic band of lipids and amino acids as well (Table 3). The band 1087 cm^{-1}, characterizing the ν(CC) vibration of lipids in disordered conformation, is two times higher in the fingertip region than the thenar (other region of the hand) or the forearm. Both bands at 1065 and 1125 cm^{-1} describe the "trans" conformation of the lipids. Therefore, the lamellar lipids are in a crystalline phase liquid in the fingertip (disordered state), whereas they are in a gel phase (mixture of trans and disordered conformation) in the thenar and forearm regions. So, this state of organization is most probably related to the anatomical site of the body. Moreover, the contribution of the band around 850 cm^{-1}, which is assigned to δ(CCH) aromatic of the tyrosine,[4,24,25] is higher in all three regions. The spectral vibration around 885 cm^{-1} is attributed to a constituent of NMF, namely the pyrrolidone 5 carboxic acid.[17,19] The proportion of this component is quite similar in both the forearm and the fingertip, and is estimated to about 15%, whereas it is higher in the thenar (about 26%) (Table 3). The 930-cm^{-1} band is the highest in the forearm, ten times in comparison with the fingertip, while approximately two times than the thenar region. The band 969 cm^{-1} is higher (35%) and downshifted to 955 cm^{-1} in the fingertip. This latter corresponds to $\rho(CH_3)$ and δ(CCH) olefinic (Table 3). The band 1001 cm^{-1} assigned to ν(CC) of phenylalanine is the most important in the forearm.

3.2 *Variations between Different Subjects in Analyzing the Same Skin Area*

Figure 5 shows spectra obtained in the same area (fingertip) from four volunteers. We can note spectral changes between the different individuals in the whole range of frequencies concerning the lipid contents, NMF content, and amino acids. Using these differences, we performed a cluster analysis and the result is shown in Fig. 6. The cluster analysis, shown by a dendogram, helps to highlight the differences observed be-

Table 2 Areas and assignments of bands resulting from curve fitting of *in vivo* Raman spectra in the frequency range 1600 to 1700 cm^{-1} (amide 1 band). $\chi^2 = 0.02^{*}10^{-2}$. The smallest χ^2, the better the deconvolution.

Wavenumber (cm^{-1})	Band area (%) forearm	Band area (%) thenar	Band area (%) fingertip	Assignment ([4,22])
1606	6.27	0.97	—	ν(CC) olefinic; phe; tyr
1612	7	3.72	18.9	—
1632	9.74	5.02	—	"out of phase" β sheet
1642	9.84	18.48 (+4 cm^{-1})	6.21 (+4 cm^{-1})	δ(OH) water
1653	37.82	52.68	39.03	α helix keratin
1660	25.87	—	—	β sheet keratin
1666	—	10.9	32.87	Random coil
1699	3.43	—	2.93	—

Table 3 Areas and assignments of bands resulting from curve fitting of *in vivo* Raman spectra in the frequency range 730 to1170 cm^{-1}. $\chi^2 = 7^{*}10^{-4}$. Assignment are referred to Refs. 4, 5, 17, 19, 24, and 25.

Wavenumber (cm^{-1})	Forearm band area (%)	Thenar band area (%)	Fingertip band area (%)	Assignment
773	4.9	8 (+2 cm^{-1})	6.64 (+10 cm^{-1})	ν(CC) ring breathing
815	7.76	3.45	—	δ(CCH) aliphatic
850	12.33	11.2	18.65	δ(CCH) aromatic
880	15.77	26.58 (+3 cm^{-1})	14.83 (+5 cm^{-1})	PCA, $\rho(CH_2)$
930	24.47	13.74 (+5 cm^{-1})	2.76 (+9 cm^{-1})	ν(CC) α-helix
969	6.88	12.06 (–2 cm^{-1})	34.6 (–14 cm^{-1})	δ(CCH) olefinic
1001	11.2	3.5	2.8	ν(CC) aromatic ring
1038	5.84	6.43	6.22	ν(CC) backbone (lipids)
1060	—	11.42 (–8 cm^{-1})	5.8	ν(CC) trans (lipids)
1087	1.9	2.5	4.8	ν(CC) random (lipids)
1125	2.1	—	1.96	ν(CC) trans conf lipids
1154	5.66	0.9 (+4 cm^{-1})	0.83	ν(CC), δ(CCH)

tween the different volunteers. For this approach, the averaged spectra from a fixed anatomical region have been used, namely the volar aspect of the forearm from seven volunteers. The volunteers were chosen with regards to their skin characteristics, which encompass a sampling from suntanned skin [Sub1(a), Sub1(b)] to a reddened skin (Sub7). The analysis was based on the fingerprint region, which includes the frequencies in the 600 to 1700 cm^{-1}. This interesting approach allowed a separation of the spectra from the same site from different subjects, even close skin, for instance, Sub2 and Sub3 (Fig. 6). The threshold of heterogeneity indicates the degree of the similarity of the compared spectra.

On the other hand, we compared two close skins (visual selection) from two women aged about 50 years old, by analyzing different anatomical sites. The spectra were obtained at the fingertip, the thenar, and the volar aspect of the forearm. In both cases, the spectra were successfully classified according to the anatomical site (data not shown).

3.3 *Variations between Different Skin Layers*

Another important issue of this experiment was the depth profiling from the surface of the skin to a fixed depth. We investigated the spectral variations at different layers from the skin surface (0 μm) to approximately 48-μm depth at the fingertip with a step of 4 μm. Figure 7 displays only the *in vivo* spectra obtained with 12 μm of increment.

Spectral changes occurred, especially in the region between 600- to 1700-cm^{-1} frequency range and around 3000 cm^{-1}. The most prominent variations were seen in the bands at 885 and 1420 cm^{-1}. Changes in water content (3100 to 3600 cm^{-1}) were less conspicuous. In contrast, the depth profile of the forearm showed similar variations to the

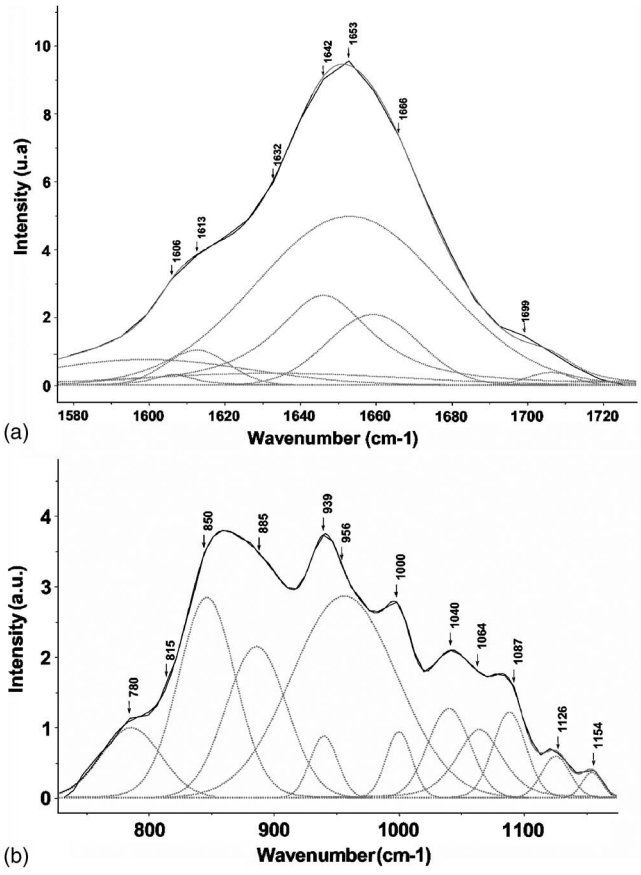

Fig. 4 Curve fitting of *in vivo* Raman spectra of skin in the frequency ranges (a) 1580 to 1720 cm^{-1}, and (b) 730 to 1170 cm^{-1}. The black and gray lines represent respectively the experimental and calculated spectra. This spectral region is area-normalized to 100% for calculation of band areas (8 and 12 bands are used). ($\chi^2 = 2^{*}10^{-4}$.) The spectra were recorded at the surface of the skin.

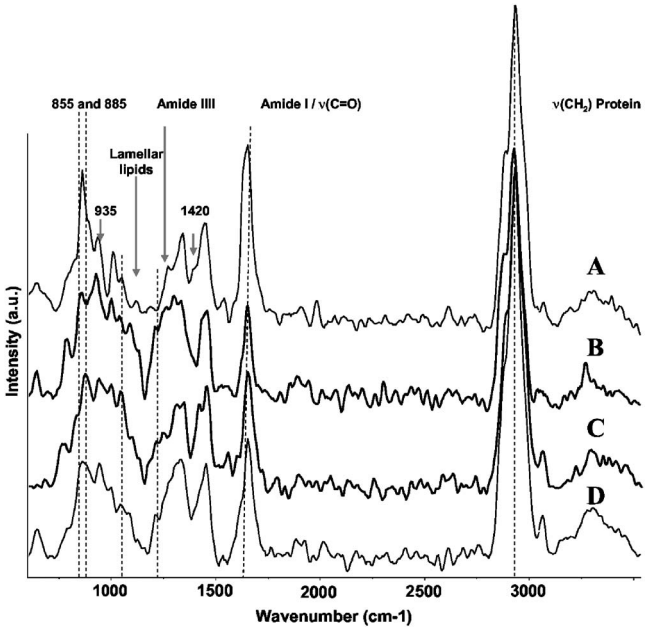

Fig. 5 *In vivo* Raman mean spectra of the *stratum corneum* at the same anatomical site (fingertip), measured at the skin surface. The spectra are from four different volunteers (a) through (d). Time collection is about 20 s. The spectra were recorded at the surface of the skin.

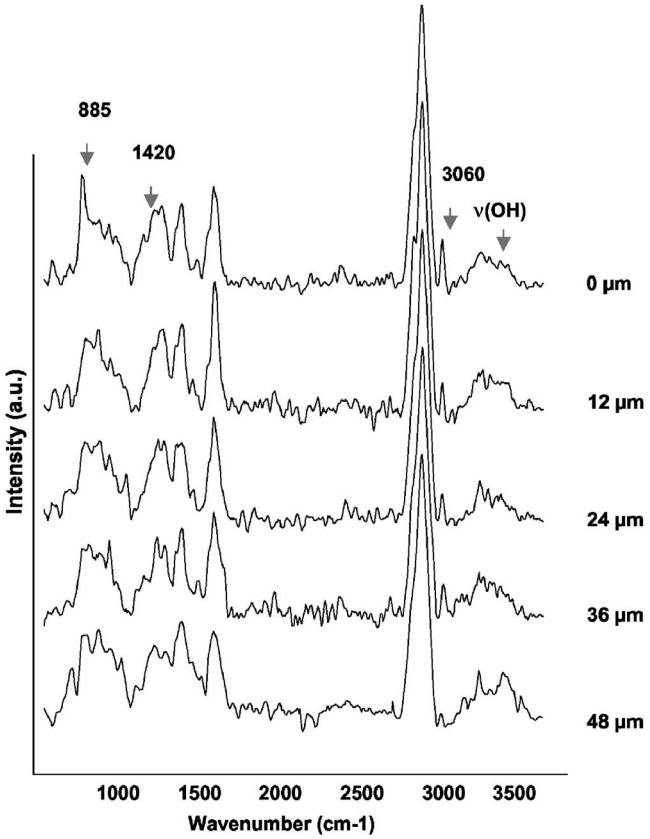

Fig. 7 *In vivo* Raman spectra of the *stratum corneum* of the fingertip in the 500 to 3600-cm^{-1} range. Raman spectra were recorded at different depths, starting from the skin surface down to 48 μm below the skin surface. Numbers to the right of the spectra indicate this depth in μm. The spectra are intensity normalized (using the 2940 cm^{-1}) assigned to protein CH stretching mode. Signal collection time: 20 s per spectrum.

fingertip in the 700- to 1700-cm^{-1} range, but also a strong increase in water content between skin surface and 28 μm deeper (Fig. 8).

4 Discussion

In this study, we demonstrated how the new confocal Raman microprobe is a powerful device for investigating molecular and structural skin composition in an *in vivo* and noninvasive way. Excellent Raman high-resolution skin spectra separate clearly the spectral variability between different spots of the same region, between different anatomical sites, intervolunteers, and between different layers. Barry, Edwards, and Williams,[4] and Williams et al.,[13] showed that there was only little variation in the spectra of the *stratum corneum* intra- and intercadavers. Gniadecka et al.[14] demonstrated *in vitro* by Fourier transform (FT) Raman that protein conformation is changed in both chronologically aged and photoaged skin compared with young skin. They based their analysis on the amide 1, amide 3 (especially 1268 cm^{-1}), and $\nu(CH_2)$ band at 2940 cm^{-1}.

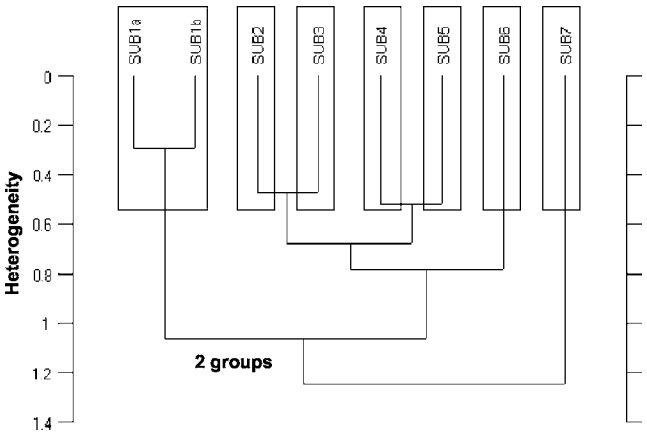

Fig. 6 Cluster analysis of *in vivo* Raman spectra taken from the same anatomical site (left forearm) from different volunteers (n=7) (Sub1 to Sub7). For the subject 1 (Sub1), we present also the right forearm [Sub1(b)]. We note two different groups with a heterogeneity level of 1.2. The analysis was performed on the 600 to 1700 cm^{-1} range, the fingerprint region.

In our investigation, we distinguished from prior studies operating on the whole spectra range from 500 to 3600 cm^{-1}. The *in vivo* human skin spectral features are in accordance with those described previously in the literature.[4] This table has been updated by adding findings from other recent reports[4,19,24,25] (see spectral vibrations marked with an asterisk in Table 1). The spectral variation between different spots of the same body region (fingertip of same subject) was evaluated (Fig. 2). In agreement with Gniadecka et al.,[14] the change in amide 1 band intensity is a consequence of water-protein interactions. Moreover, we have detected other spectral changes related to the band at 855 cm^{-1}, assigned to δ(CCH) of aromatic of tyrosine, and which reveals a hydrophilic environment. Along these lines, we suggest that these changes

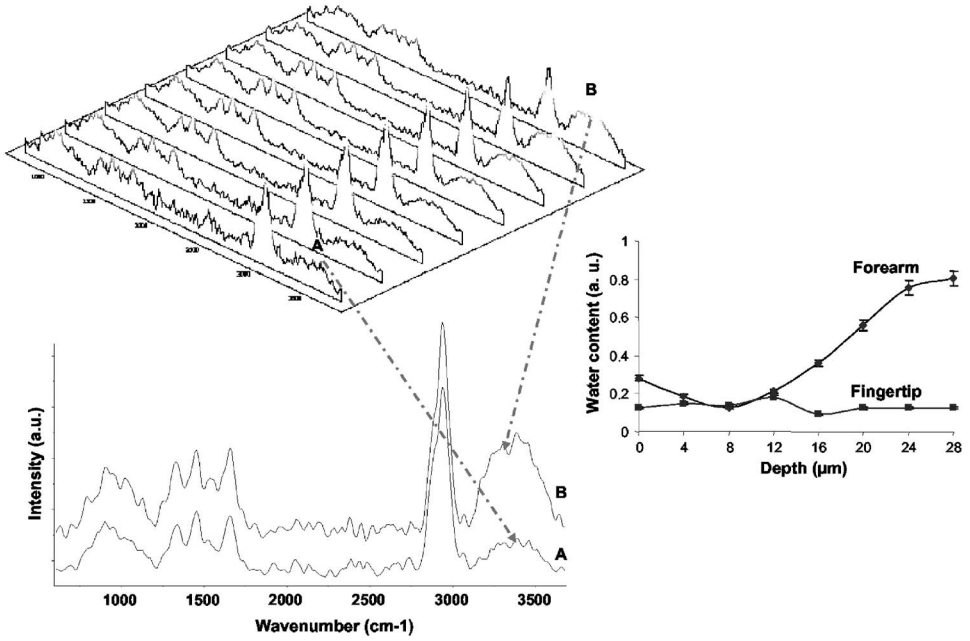

Fig. 8 Comparison of *in vivo* spectra obtained at the forearm at different depths: (a) 0 μm, and (b) 28 μm. The acquisition time is 20 s per spectrum. An increase in water content is observed for 28 μm. The comparison of the water content to 28 μm deep into the skin is represented through a curve; the upper is about the forearm, whereas the lower concerns the fingertip. This ratio consists of OH (water)/CH_3 (proteins).[36] The error bars plotted represent 5% in the determination of the intensity ratio.

are due to the presence of sweat, which is mainly composed of lactate (band at 855 cm^{-1}) and urea that can modify the environment. Consequently, this Raman probe enables the detection of sweat and its effect on skin composition.

Our analysis between different anatomical sites (fingertip, thenar, and forearm from same subject) showed differences in amide 1 (1600 to 1700 cm^{-1}) and amide 3 (1240 to 1300 cm^{-1}), regions characteristic of keratin (major protein), which predominantly adopts an α-helical conformation.[4] More specifically, the results of curve fitting indicate the presence of different secondary protein conformation. We distinguish α-helix conformation mostly at 1653 cm^{-1}, β sheet conformation featured at 1666 cm^{-1}, and random coil configuration at 1660 cm^{-1}. Moreover, the content of these different secondary structures varies following the anatomical site. Indeed, according to the curve fitting, the forearm presents a mixture of organized structures, namely 38% of α helix and 26% of β sheet (Table 2). In contrast, the fingertip region displays about the same amount of structured protein (39% α-helix form) and unstructured protein form (33% random coil). These findings support the view that the proteins are more highly organized in the forearm than in the fingertip. The deconvolution of this amide 1 band also enhances the hidden vibration of the water bending mode around 1642 cm^{-1}. The proportion of this band is clearly linked to the hydration of the *stratum corneum* of the anatomical site. Thus, the water content is about 18% in the thenar compared to 10% in the forearm and 6% in the fingertip (Table 2). We make evident here an inhomogeneous distribution of water, depending on the different anatomical sites. This allowed a better understanding of protein change, previously unexplained.

The curve-fitting analysis of the 730 to 1170 cm^{-1} reveals the lamellar organization of lipids in all studied anatomical sites (see Table 3). The bands at 1060, 1125, and 1296 cm^{-1} are characteristic of ceramides 1 (major lipids component of the *stratum corneum*).[3] The first two bands are attributed to the all-trans conformation (gel phase) of the acyl backbone in lipids, whereas the band at 1087 cm^{-1} is mainly due to the gauche conformation (liquid crystal phase).[26] This indicates markedly a lipid structure in a gel phase for the forearm and the thenar regions in contrast to a liquid crystalline phase in the fingertip region, which is a disorganized state. In addition, the intensity of the band at 2885 cm^{-1} corresponding to asymmetric CH_2 stretching of lipids is more prominent in the forearm than in other anatomical sites (Fig. 3). Thus, this feature suggests not only a qualitative difference in lipids content but a quantitative one as well, relevant to the anatomical site.

NMF are known to be efficient humectants, especially in the *stratum corneum* layer.[6] They comprise a highly water soluble and hygroscopic mixture of amino acids, and the major components are serine, PCA, and glycine.[6,27,28] As described earlier, the intense 855-cm^{-1} band indicates a chemical hydrophilic environment of the tyrosine in the three analyzed regions. This provides additional insights into the behavior of different components of the skin, like tyrosine and lactate. The intensity change of the band at 1420 cm^{-1} described as originating from glycine, serine, and alanine (constituent of the NMF) and that at 885 cm^{-1} (PCA of NMF),[19] reveals that the NMF molecular composition of the *stratum corneum* varies according to the anatomical sites (Fig. 3).

We established that different anatomical sites differ from their NMF constituent, lipids, and secondary conformation of

proteins, which is in total agreement with the results obtained with different Raman systems and ATR-FTIR investigations.[17,29] Accordingly, the molecular variation of the *stratum corneum* is closely related to the physical properties of the skin. The forearm *stratum corneum* presents not only more organized proteins but also more organized lipids as well, compared to the fingertip *stratum corneum*. This better arrangement implies that the barrier function is more efficient within the forearm, despite its smaller thickness, than within the fingertip.

Figure 5 exposed unequivocally similar variations of NMF components, lipids, and proteins between different individuals using measurements of the same region. The intersubject variations are explained partly by their lipid (ceramides 1) and protein contents.[30] The protein variation results from different levels of maturation and natural hydration of the skin between different subjects. The observed NMF changes are consistent with a different state of the protein proteolysis pattern, the filaggrin protein being the main precursor of the NMF. Hence, NMF spectral features can be used as a biochemical marker to evaluate dry skin or the physical properties of the *stratum corneum*, as has been described by other methods.[31,32] The cluster analysis based on the spectral window 600 to 1700 cm^{-1} allowed a classification of the spectra of the *stratum corneum* acquired at the volar aspect of the forearm from different volunteers. We distinguish two extreme cases in the dendogram[33] related to the suntanned or matt skin [Sub1(a) and Sub1(b)] and the reddened skin (Sub7) (Fig. 6). This original approach can offer a quick and noninvasive way of classifying the skin in a given area and according to body area.

The depth profiles of the *stratum corneum* were carried out from the surface to approximately 50 μm deep in the fingertip (Fig. 7). Spectral variations were observed between 800 to 900 cm^{-1} and at the 1420 cm^{-1} band (NMF). The water content of a fingertip does not vary from the surface of the skin to a depth of 50 μm, because this region lies within the 100 μm thickness of the *stratum corneum* at this site. In contrast at the level of the forearm, water content increases very quickly from the surface to about 28 μm in-depth. This increase discloses the *stratum corneum/stratum granulosum* interface (Fig. 8),[34–36] taking into consideration that the thickness of the *stratum corneum* is about 10 to 15 μm for the forearm. Changes in water content according to the depth are associated with changes in the molecular composition of *stratum corneum*, especially regarding NMF and lipid contents.[19,29]

5 Conclusion

This study clearly demonstrates the availability of the *in vivo* confocal Raman microprobe for rapid, noninvasive, and nondestructive molecular characterization of skin with respect to various anatomical sites, various layers (outermost and deeper) of the skin, and between individuals. Additionally, this probe reveals the water gradient from the surface to several microns below the skin surface. Thus, monitoring the percutaneous penetration of active molecules (drug, cosmetics), elucidating their interaction with skin components, their *in vivo* kinetics, and better understanding of the barrier function are feasible with this *in vivo* confocal Raman microprobe. Indeed, both qualitative and quantitative information are available.

Further ergonomics improvement of the *in vivo* confocal Raman microprobe will offer an easier access to other anatomical sites, for example, leg, forehead, or cheek. With this point of view, a *in vivo* confocal Raman microprobe can generate useful information concerning the skin in pharmaceutical and dermatological approaches. The strong features of this probe are the widespread applications, the noninvasive and nondestructive aspects, and the flexibility of the ergonomics.

References

1. A. S. Michaels, S. K. Chandrasekaran, and J. E. Shaw, "Drug permeation through human skin: Theory and *in vitro* experimental measurement," *J. Am. Inst. Chem. Eng.* **21**, 985–996 (1975).
2. S. Grayson and P. M. Elias, "Isolation and lipid biochemical characterization of *stratum corneum* membrane complexes: implications for the cutaneous permeability barrier," *J. Invest. Dermatol.* **78**(2), 128–135 (1982).
3. P. W. Wertz and D. T. Downing, "Glycolipids in mammalian epidermis: structure and function in the water barrier," *Science* **217**(4566), 1261–1262 (1982).
4. B. W. Barry, H. G. M. Edwards, and A. C. Williams, "Fourier transform Raman and infrared vibrational study of human skin: Assignment of spectral bands," *J. Raman Spectrosc.* **23**, 641–645 (1992).
5. A. N. C. Anigbogu, A. C. Williams, B. W. Barry, and H. G. M. Edwards, "Fourier transform Raman spectroscopy of interactions between the penetration enhancer dimethyl sulfoxide and human *stratum corneum*," *Int. J. Clin. Pharmacol.* **125**, 265–282 (1995).
6. A. V. Rawlings, I. R. Scott, C. R. Harding, and P. A. Bowser, "*Stratum corneum* moisturization at the molecular level," *J. Invest. Dermatol.* **103**, 731–741 (1994).
7. H. Tagami, M. Ohi, K. Iwatsuki, Y. Kanamaru, M. Yamada, and B. Ichijo, "Evaluation of the skin surface hydration *in vivo* by electrical measurement," *J. Invest. Dermatol.* **75**, 500–507 (1980).
8. D. R. Bommannan, R. O. Potts, and R. H. Guy, "Examination of *stratum corneum* barrier function *in vivo* by infrared spectroscopy," *J. Invest. Dermatol.* **95**, 403–408 (1990).
9. K. Wichrowski, G. Sore, and A. Khaiat, "Use of infrared spectroscopy for *in vivo* measurement of the *stratum corneum* moisturization after application of cosmetic preparations," *Int. J. Cos. Sci.* **17**, 1–11 (1995).
10. F. Pirot, Y. N. Kalia, A. L. Stinchcomb, G. Keating, A. Bunge, and R. H. Guy, "Characterization of the permeability barrier of human skin *in vivo*," *Proc. Natl. Acad. Sci. U.S.A.* **94**, 1562–1567 (1997).
11. R. O. Potts, D. B. Guzek, H. H. Harris, and J. E. Mckie, "A noninvasive, *in vivo* technique to quantitatively measure of water concentration of the *stratum corneum* using attenuated total-reflectance infrared spectroscopy," *Arch. Dermatol. Res.* **277**, 489–495 (1985).
12. G. W. Lucassen, G. N. A. Van Veen, and J. A. J. Jansen, "Band analysis of hydrated human skin *stratum corneum* ATR-FTIR spectra *in vivo*," *J. Biomed. Opt.* **3**(3), 267–280 (1998).
13. A. C. Williams, B. W. Barry, H. G. M. Edwards, and D. W. Farwell, "A critical comparison of some Raman spectroscopic techniques for studies of human *stratum corneum*," *Pharm. Res.* **10**, 1642–1647 (1993).
14. M. Gniadecka, O. F. Nielsen, S. Wessel, M. Heidenheim, D. H. Christensen, and H. C. Wulf, "Water and protein structure in photoaged and chronically aged skin," *J. Invest. Dermatol.* **111**, 1129–1133 (1998).
15. B. Schrader, B. Dippel, S. Fendel, S. Keller, T. Lochte, M. Riedl, R. Schulte, and E. Tatsch, "NIR FT Raman spectroscopy-a new tool in medical diagnosis," *J. Mol. Struct.* **408/409**, 23–31 (1997).
16. M. G. Shim and B. C. Wilson, "Development of an *in vivo* Raman spectroscopic system for diagnostic applications," *J. Raman Spectrosc.* **28**, 131–142 (1997).
17. P. J. Caspers, G. W. Lucassen, R. Wolthuis, H. A. Bruining, and G. J. Puppels, "*In vitro* and *in vivo* Raman spectroscopy of human skin," *Biospectroscopy* **4**, S31–39 (1998).
18. P. J. Caspers, G. W. Lucassen, and G. J. Puppels, "Combined in vivo confocal Raman spectroscopy and confocal microscopy of human skin," *Biophys. J.* **85**, 572–580 (2003).

19. P. J. Caspers, G. W. Lucassen, E. A. Carter, H. A. Bruining, and G. J. Puppels, "*In vivo* confocal Raman microspectroscopy of human skin: noninvasive determination of molecular concentration profiles," *J. Invest. Dermatol.* **116**(3), 434–442 (2001).
20. P. R. Griffiths and J. H. Haseth, "A series of monographs on analytical chemistry and its applications," in *Chemical Analysis*, P. J. Elving, J. D. Winefordner, and I. M. Kolthoff, Eds., Vol. **83**, Wiley, New York (1986).
21. G. Sockalingum, W. Bouhedja, P. Pina, P. Allouch, C. Mandray, R. Labias, J. M. Millot, and M. Manfait, "ATR-FTIR spectroscopic investigation of imipenem-susceptible and resistant pseudomonas aeruginosa isogenic strains," *Biochem. Biophys. Res. Commun.* **232**, 240–246 (1997).
22. A. C. Williams, H. G. M. Edwards, and B. W. Barry, "Raman spectra of human keratotic biopolymers: Skin, callus, hair and nail," *J. Raman Spectrosc.* **25**, 95–98 (1994).
23. M. Byler and H. Susi, "Examination of the secondary structure of proteins by deconvolved FTIR spectra," *Biopolymers* **25**, 469–487 (1986).
24. A. Rodriguez-Casado, S. D. Moore, P. E. Prevelige Jr., and G. J. Thomas Jr., "Structure of bacteriophage P22 portal protein in relation to assembly: investigation by Raman spectroscopy," *Biochemistry* **40**, 13583–13591 (2001).
25. C. Xiao, C. R. Flach, C. Marcott, and R. Mendelsohn, "Uncertainties in depth determination and comparison of multivariate with univariate analysis in confocal Raman studies of a laminated polymer and skin," *Appl. Spectrosc.* **58**(4), 382–389 (2004).
26. G. S. Pilgram, A. M. Van Pelt, F. Spies, J. A. Bouwstra, and H. K. Koerten, "Cryoelectron diffraction as a tool to study local variations in the lipid organization of human *stratum corneum*," *J. Microsc.* **189**, 71–78 (1998).
27. I. Horii, K. Kawasaki, J. Koyama, Y. Nakayama, N. Nakajima, K. Okazaki, and M. Seiji, "Histidine-rich protein as a possible origin of free amino acids of *stratum corneum*," *J. Invest. Dermatol.* **10**, 25–33 (1983).
28. J. Tabachnick and J. H. Labadie, "Studies on the biochemistry of epidermis. IV. The free amino acids, ammonia urea, and pyrrolidone carboxylic acid content of conventional and germ-free albino guina pig epidermia," *J. Invest. Dermatol.* **54**, 24–31 (1970).
29. L. Brancaleon, M. P. Bamberg, T. Sakamaki, and N. Kollias, "Attenuated total reflection-Fourier transform infrared spectroscopy as a possible method to investigate biophysical parameters of *stratum corneum in vivo*," *J. Invest. Dermatol.* **116**(3), 380–386 (2001).
30. L. Knudsen, C. K. Johansson, P. A. Philipsen, M. Gniadecka, and H. C. Wulf, "Natural variations and reproductibility of *in vivo* near-infrared Fourier transform Raman spectroscopy of normal human skin," *J. Raman Spectrosc.* **33**, 574–579 (2002).
31. J. Koyama, I. Horii, K. Kawasaki, Y. Nakayama, Y. Morikawa, and T. Mitsui, "Free amino acids of *stratum corneum* as a biochemical marker to evaluate dry skin," *J. Soc. Cosmet. Chem.* **35**, 183–195 (1984).
32. N. Nakagawa, S. Sakai, M. Matsumoto, K. Yamada, M. Nagano, T. Yuki, Y. Sumida, and H. Uchiwa, "Relation ship between NMF (lactate and potassium) content and the physical properties of the *stratum corneum* in healthy subjects," *J. Invest. Dermatol.* **122**, 755–763 (2004).
33. C. Sandt, G. D. Sockalingum, D. Aubert, H. Lepan, C. Lepouse, M. Jaussaud, A. Leon, J. M. Pinon, M. Manfait, and D. Toubas, "Use of Fourier-transform infrared spectroscopy for typing Candida albicans strains isolated in intensive care unit," *J. Clin. Microbiol.* **41**(3), 954–959 (2003).
34. T. Von Ziglinicki, M. Lindberg, G. M. Roomans, and B. Forslind, "Water and ion distribution profiles in human skin," *Acta Derm Venereol* **73**, 340–343 (1993).
35. R. R. Warner, M. C. Myers, and D. A. Taylor, "Electron probe analysis of human skin: determination of the water concentration profile," *J. Invest. Dermatol.* **90**, 218–224 (1988).
36. N. J. Bauer, J. P. Wicksted, F. H. Jongsma, W. F. March, F. Hendrikse, and M. Motamedi, "Noninvasive assessment of the hydration gradient across the cornea using confocal Raman spectroscopy," *Invest. Ophthalmol. Visual Sci.* **39**, 831–835 (1998).